Science of Remote Sensing 12 (2025) 100302

Contents lists available at ScienceDirect

Science of Remote Sensing

journal homepage: www.sciencedirect.com/journal/science-of-remote-sensing

Mapping herbivore-accessible biomass across a heterogeneous mountain landscape using multisensor high-resolution UAV data

Annika M. Zuleger [a,b,*], Martina M. Viti [a,b], Luise Quoss [a,b], Filipe S. Dias [c,d,e,f], Luís Borda-de-Água [a,b,d,f], Miguel N. Bugalho [f], Henrique M. Pereira [a,b,e]

[a] Institute of Biology, Martin Luther University Halle-Wittenberg, Halle (Saale), Germany
[b] German Centre for Integrative Biodiversity Research (iDiv) Halle-Jena-Leipzig, Leipzig, Germany
[c] CIBIO, Centro de Investigação em Biodiversidade e Recursos Genéticos, InBIO Laboratório Associado, Campus de Vairão, Universidade do Porto, Vairão, Portugal
[d] CIBIO, Centro de Investigação em Biodiversidade e Recursos Genéticos, InBIO Laboratório Associado, Instituto Superior de Agronomia, Universidade de Lisboa, Lisbon, Portugal
[e] BIOPOLIS Program in Genomics, Biodiversity and Land Planning, CIBIO, Campus de Vairão, Vairão, Portugal
[f] Center for Applied Ecology "Prof. Baeta Neves" (CEABN-InBIO), School of Agriculture, University of Lisbon, Lisbon, Portugal

ARTICLE INFO

Keywords:
Herbivore-accessible biomass
UAV remote sensing
NDVI
LiDAR
Generalized Additive Mixed models (GAMMs)
Vegetation modeling
Heterogeneous landscapes

ABSTRACT

Herbivore-accessible biomass (HAB), defined as aboveground biomass under 2 m, including leaves and soft branches, is a key metric for understanding ecosystem function, but remains poorly quantified. We estimated HAB across diverse habitats in the Peneda-Gerês National Park using high-resolution NDVI, LiDAR, topography and field data. Generalized Additive Mixed Models (GAMMs) revealed habitat-specific effects of NDVI and vegetation height, as well as terrain, and structural metrics across plant types. Models were evaluated using hold-out cross-validation on a 20 % subset of the field data. The total HAB model performed well (Deviance Explained = 0.77, $RMSE_{20}$ = 172.38 g/m^2), while the shrub model performed slightly worse (Deviance Explained = 0.71, $RMSE_{20}$ = 410.21 g/m^2), and the herbaceous model exhibited a moderate fit and accuracy (Deviance Explained = 0.69, $RMSE_{20}$ = 34.25 g/m^2). Average total HAB was 1.31 ± 0.83 tons/ha, dominated by shrubs (1.02 tons/ha) compared to herbaceous HAB (0.14 tons/ha). HAB density varied by habitat, highest in shrublands (up to 1.83 ton/ha) and lowest in oak forests (0.85 tons/ha), while agricultural areas supported the most herbaceous HAB (0.68 tons/ha). These values are substantially lower than shrub biomass estimates reported in other studies (e.g., up to 30 tons/ha), reflecting our focus on live biomass <2 m. Prediction uncertainty was low (CV: 22–34 %), improving on other studies reporting up to 190 %, and highlighting the strength of combining spectral and structural data for fine-scale forage estimation. This study provides the first spatially explicit HAB estimates for the area, supporting herbivore ecology and management.

1. Introduction

Aboveground plant biomass ('AGB' or 'biomass' hereafter) is a key ecological metric, particularly in shrubland and grassland ecosystems, where it captures information on carbon storage, ecosystem productivity, habitat structure, vegetation dynamics, and overall ecosystem health (Aranha et al., 2020; Bazzo et al., 2023; Li et al., 2017). Estimating herbaceous and shrub biomass is essential for assessing fuel loads, tracking changes in native species, and understanding the impacts of landscape changes (Li et al., 2017). Grasslands and shrublands play a central role in global carbon cycles, and their biomass responds rapidly to shifts in precipitation, temperature, and disturbance regimes, making them sensitive indicators of climate change (Gorissen et al., 2004; Lei et al., 2016). Additionally, plant biomass can provide information on forage availability, which governs herbivore populations, species interactions, trophic dynamics and rangeland management (Riquelme et al., 2022).

Yet, estimating AGB, especially in shrublands and grasslands, presents significant challenges. Traditional methods, including in situ techniques like harvesting and visual estimations, rely on exhaustive field sampling, which is labor-intensive, time-consuming, and impractical for large-scale applications. Remote sensing offers a more efficient alternative, especially when integrated with field data, enabling scalable and reliable AGB estimation across diverse landscapes. However, shrub-

* Corresponding author. Institute of Biology, Martin Luther University Halle-Wittenberg, Halle (Saale), Germany.
E-mail address: annika_mikaela.zuleger@idiv.de (A.M. Zuleger).

https://doi.org/10.1016/j.srs.2025.100302
Received 31 March 2025; Received in revised form 29 August 2025; Accepted 3 October 2025
Available online 3 October 2025

and herbaceous-dominated systems introduce unique difficulties due to the structural complexity of low-growing vegetation with dense, heterogeneous cover (Pervin et al., 2022). In these ecosystems, shrubs and grasses often form vertically overlapping canopies, complicating the separation of individual vegetation components using remote sensing (Pervin et al., 2022). Additionally, herbaceous and woody plants exhibit similar light reflectance patterns, leading to spectral confusion that limits the ability of optical sensors to differentiate between them (Burai et al., 2015). Consequently, distinguishing and accurately quantifying biomass from these components remains a key challenge.

Nevertheless, methods combining field data collection with remote sensing techniques, particularly those utilizing the Normalized Difference Vegetation Index (NDVI) and Light Detection and Ranging (LiDAR) metrics, have become increasingly popular in recent years. Numerous studies have shown that remote sensing data, such as NDVI and LiDAR metrics, are highly effective in estimating AGB in a variety of landscapes, such as different types of forest and woodland ecosystems (Campbell et al., 2021; Ceballos et al., 2015; Estornell et al., 2012; Fassnacht et al., 2014; Narine et al., 2019), shrublands (Aranha et al., 2020; Chang and Shoshany, 2016; Fernández-Alonso et al., 2022; Li et al., 2017; Zhao et al., 2021) or grasslands (Bazzo et al., 2023; Lussem et al., 2019; Zhang et al., 2018; Zhao et al., 2021).

NDVI provides a reliable measure of vegetation productivity and density by capturing differences in light absorption and the reflectance of near-infrared light, making it a useful indicator of photosynthetic activity and vegetation cover (Estornell et al., 2012; Fassnacht et al., 2014; Fernández-Alonso et al., 2022; Narine et al., 2019). However, despite its widespread use in vegetation monitoring, NDVI has limitations in biomass estimation, particularly in forest habitats, due to signal saturation at high biomass levels (Bazzo et al., 2023; Greaves et al., 2016). Moreover, NDVI values do not distinguish between vegetation types (e.g. forests, shrublands or grasslands), but instead only reflect vegetation cover density (Aranha et al., 2020). As a result, additional data on structural metrics are necessary.

These structural metrics can be provided through LiDAR, which offers detailed three-dimensional measurements of vegetation structure, enabling multiscale AGB estimates and critical insights into habitat structure and landscape-level dynamics (Lefsky et al., 2002; Li et al., 2017). Through the emission of airborne laser pulses, LiDAR can capture important predictors such as vegetation height, canopy cover, volume, and surface roughness - metrics that are particularly useful for detecting low-stature shrubs and structural heterogeneity (Campbell et al., 2021; Estornell et al., 2012; Fassnacht et al., 2014; Fernández-Alonso et al., 2022; Lefsky et al., 2002). It has been successfully implemented not only in AGB estimation, but also to assess post-disturbance structural changes and biodiversity patterns (Ceballos et al., 2015; Fernández-Alonso et al., 2022). Still, high-resolution data are often required to detect fine-scale variation in open habitats, and the effectiveness of LiDAR can vary with vegetation density and landscape complexity (Campbell et al., 2021; Greaves et al., 2016).

Recent advances in remote sensing technologies, particularly through drones and unmanned aerial vehicles (UAVs), have revolutionized ecological and environmental monitoring (Bazzo et al., 2023; Manfreda et al., 2018). Although UAV systems lack the broad spatial coverage of satellite imagery, they offer superior spatial and temporal resolution at significantly lower costs for smaller areas of interest (Bazzo et al., 2023; Manfreda et al., 2018). Therefore, UAVs have emerged as powerful tools for measuring biophysical parameters, providing cost-effective, scalable, and repeatable solutions. Equipped with advanced sensors such as multispectral, hyperspectral, and LiDAR systems, UAVs bridge the gap between field observations and traditional air- and space-borne remote sensing, enabling high-resolution data collection with remarkable precision and flexibility (Manfreda et al., 2018). These capabilities allow for comprehensive assessment of AGB and other ecological metrics across vast, inaccessible areas, making them invaluable for ecological research and resource management.

Despite these advances, most remote sensing-based AGB studies focus on woody plant biomass in forests, such as those in tropical or boreal regions (Campbell et al., 2021), or are limited to specific vegetation strata, such as trees, shrubs, or grasses (e.g. Anderson et al., 2018; Aranha et al., 2020; Estornell et al., 2012; Li et al., 2017; Vega et al., 2022; Wang et al., 2007). Additionally, traditional AGB estimation approaches typically integrate total vegetation height and structure across the entire canopy, often emphasizing upper-canopy layers.

Our study addresses this gap by estimating herbivore-accessible biomass (HAB) across a heterogeneous landscape that encompasses multiple different habitat types and vegetation strata. We defined HAB as the portion of aboveground biomass below 2 m that includes both leaves and edible, non-lignified branches accessible to large herbivores within the study area. This definition excludes woody structural components not typically consumed, as well as all biomass above a browsing line of 2 m (maximum height the target herbivores can feed on the tree and shrub canopy), focusing instead on the plant material that realistically contributes to herbivore diets. Field data collection and subsequent modeling were therefore limited to biomass within this lower stratum. For taller shrubs, only the portion of the plant below 2 m was sampled and used in model training. Similarly, remote sensing predictors were interpreted in relation to this specific vegetation layer, ensuring that both sampling and modeling targeted only the biomass realistically available to herbivores. This represents a conceptual and analytical shift from total AGB estimation, focusing the approach to trophic accessibility rather than total productivity.

We modeled and mapped both herbaceous and shrub HAB across a heterogeneous part of the Peneda-Gerês National Park in Portugal using a combination of field sampling and remote sensing data. Field sampling was conducted across diverse habitat types using transects, while remote sensing data included spectral, structural, and, topographic metrics, as well as land-cover information. By integrating these data into a unified model, we aim to (1) improve the scalability and efficiency of biomass estimation across heterogeneous mountain landscapes, and to (2) provide a framework for the estimation of HAB, offering insights that are essential for conservation and natural resource management.

2. Methods

2.1. Study area

The study was conducted in the parishes of Castro Laboreiro and Lamas de Mouro in the Peneda-Gerês National Park in northern Portugal (Fig. 1). The area is shaped by rural depopulation and agricultural land abandonment driving ecological succession over the past 60 years (van der Zanden et al., 2018). Especially in the region surrounding Castro Laboreiro where historically agro-pastoral activities were common (van der Zanden et al., 2018), socio-economic changes led to a large population decline (Lourenço and Quental, 2007; Rodrigues, 2010). The resulting agricultural abandonment led to changes in the vegetation structure, with former agricultural lands and pastures transitioning first to shrublands and eventually to oak forests. This transition has likely increased AGB due to the expansion of shrub cover and woody vegetation, with implications for carbon sequestration, fuel loads, and habitat structure (Castro and Freitas, 2009). Additionally, this process, often referred to as passive or ecological rewilding, has been associated with an increase in the densities of several wildlife species (Pereira and Navarro, 2015).

Today, the region comprises a mosaic of diverse habitats, including extensive shrublands, small agricultural pastures, oak and pine forests in the valley and rocky outcrops at higher elevations (Fig. S3). Generally, the land cover is dominated by open spaces with minimal vegetation, where vegetation degradation and soil erosion, partly driven by agricultural land conversion, are leading to transitions toward sparse vegetation or bare rock (Lourenço and Quental, 2007). Shrublands are mostly composed of Ericaceae (*E. umbellata*, *E. australis*, *E. cinerea*,

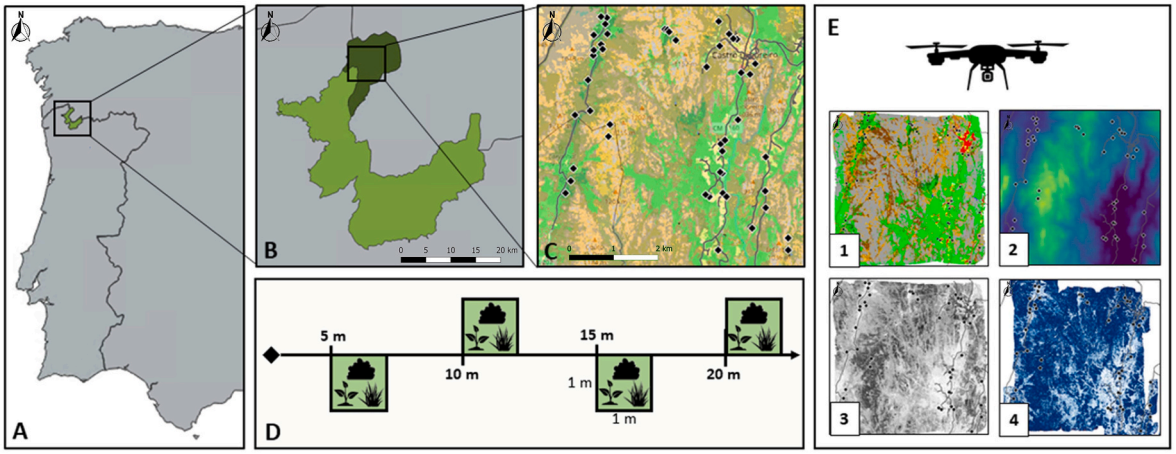

Fig. 1. Study Location and Sampling Design. A) Location of the Peneda-Gerês National Park in Portugal. B) Parishes of Castro Laboreiro and Lamas de Mouro in the National Park. C) Sampling Locations and habitat types within the study area. D) Field Sampling Design. E) Remote-Sensing metrics used for modeling: 1. habitat types obtained from Random Forest Classification. 2. Topographic information (Elevation, Slope, Aspect). 3. NDVI. 4. LiDAR metrics (Aboveground Height, Canopy Cover, Vertical Point Cloud Densities).

E. arborea, and *Calluna vulgaris*) and Leguminosae (*Ulex* spp., *Cytisus* spp., *Pterospartum tridentatum*). The valleys are occupied by oak forests of Quercus (*Q. pyrenaica* and *Q. robur*) and Betula (*B. pendula* and *B. pubescens*), as well as pine forests of *Pinus sylvestris* and *Pinus pinaster*. Overall, the National Park protects 24 habitat types under the Habitats Directive, with *Galicio-Portuguese oak woods* and *European dry heaths* being the most significant (European Nature Information System, EUNIS).

The study area is located in a climatic transition zone, where Mediterranean and Atlantic influences create a temperate Mediterranean climate (Carvalho-Santos et al., 2018; van der Zanden et al., 2018). Winters are cold and rainy, with an average temperature of 6.6 °C, while summers are warm, averaging 17.3 °C (own data). The region experiences 1–2 dry months in summer, with an overall mean annual temperature of 11.6 °C between 2015 and 2022 (own data). Annual precipitation is typically around 1500 mm, sometimes reaching 3000 mm at higher elevations (Carvalho-Santos et al., 2018).

2.2. Remote sensing data

We used a combination of environmental predictors derived from remote sensing encompassing three distinct domains: (1) spectral metrics, such as the Normalized Difference Vegetation Index (NDVI); (2) structural variables derived from LiDAR data; and (3) topographic indices obtained from digital elevation models (DEMs). Additionally, land-cover information was obtained through automatic classification using RGB, NDVI and LiDAR data as input (Supplemental Material S4).

2.2.1. Topography

A high-resolution digital surface model (DSM) was generated from imagery collected in 2015 over a 22.8 km^2 area using a SenseFly eBee Classic drone equipped with a Canon PowerShot ELPH 110 HS-NIR camera (Fig. S3). The drone operated at a 110 m altitude, achieving a spatial resolution of 13.4 cm. The imagery was processed with Post Flight Terra 3D (version 3.4.46, Pix4D, 2011) to generate a 2.5 m resolution DSM by extracting and matching key points using the Scale-Invariant Feature Transform (SIFT) algorithm (Lowe, 1999), calibrating the camera, aligning images into a sparse point cloud, and reconstructing 3D terrain structure through multi-view stereo techniques. From the DSM a Digital Terrain Model (DTM) was produced by filtering out non-ground points. Slope and aspect data were derived from the DTM using the Raster Terrain Analysis Plugin in QGIS (Version 3.24.2, Fig. S3).

2.2.2. Spectral data

NDVI metrics were derived from imagery captured in May 2023 using a SenseFly eBee X drone equipped with a Parrot Sequoia + Camera (Sequoia_4.0_1280x960, Fig. S3), collecting data in four discrete spectral bands (green, red, red-edge, and near-infrared), as well as RGB imagery in the visible spectrum. Flight planning was conducted using the eMotion flight control software (AgEagle, 2023), dividing the survey area into nine grid cells, each flown separately. Flights were conducted at a fixed height of 127 m above elevation using the 2015 DTM as the reference surface. This resulted in a spatial resolution of 25.9 cm for the spectral bands and 7 cm for the RGB-imagery.

Georeferencing was performed in eMotion, and further processing was conducted in Pix4Dmapper (Pix4D, 2023). This included radiometric calibration to correct for sensor and lighting variations, image alignment for spatial consistency, and the generation of NDVI values and orthomosaics.

2.2.3. LiDAR data

LiDAR data were collected in May and September 2024 using a DJI Zenmuse L2 camera mounted on a DJI Matrice 350 RTK drone. Flights were conducted at approximately 220 m above ground level (AGL), capturing RGB imagery at 6 cm resolution and a LiDAR point cloud with a density of 42 points/m^2. The ASTER Global Digital Elevation Model (GDEM, version 3, NASA/METI/AIST/Japan Spacesystems And U. S./Japan ASTER Science Team, 2019) served as the altitude reference for ground level. As with NDVI data collection, flight planning was carried out in nine grid cells. To enhance spatial accuracy, real-time kinematic (RTK) positioning was used, with correction signals obtained from the Ntrip (Networked Transport of RTCM via Internet Protocol) broadcaster from the Federal Agency for Cartography and Geodesy (BKG: Bundesamt für Kartographie und Geodäsie). During the flights, we used the data from the station in Vigo, Spain (VIGO00ESP0) of the euref-ip.net GNSS Streaming Server (http://euref-ip.net/home). This precise positioning enabled the collection of high-quality LiDAR data suitable for detailed vegetation analysis. The data were processed in DJI Terra (DJI, 2019) to convert the proprietary point cloud format into an LAS point cloud (ASPRS, 2019). Additionally, DJI Terra colorized the LiDAR point cloud using RGB imagery and performed ground point classification to differentiate between ground and non-ground points, such as low-shrub and herbaceous vegetation, effectively. The 'Steep Slope' ground type setting was selected, which adjusts classification parameters, such as a 10-degree iteration angle and a 0.7-m iteration distance, to improve ground point identification in mountainous or rugged terrain.

Vegetation metrics were extracted from the point cloud using QGIS (3.38.3) and the *lidR* package in R (Roussel and Auty, 2016). These included aboveground height (AGH) and canopy cover (CC), calculated as mean, maximum and minimum values (Fig. S2). Canopy cover was defined as the proportion of points ≥2 m relative to all height points. Additionally, we computed metrics specifically aimed at vegetation below 2 m to address the focus of this study. We extracted vertical relative point density (VRD) and percent of vegetation (PH) across height intervals based on vegetation height data collected during field sampling (e.g., 0–0.25 m for low herbaceous biomass, 0.25–0.5 m for tall herbaceous and low shrub biomass, 0.5–1 m for shrubs, and 1–2 m for tall shrubs; Fig. S3). VRD quantifies the proportion of LiDAR returns within each height interval relative to all returns below 2 m, while PH represents the percentage of returns in each interval relative to all returns within a pixel. Both metrics provide detailed insight into the vertical vegetation structure, especially within the lower strata below 2 m. Including these metrics in the model ensures estimates focus on herbivore-accessible vegetation, distinguishing this study from traditional biomass approaches. The CC, VRD and PH metrics were derived directly from the point cloud at 10 cm spatial resolution using the *lidR* package. AGH was obtained from a digital height model (DHM) raster calculated from the point clouds using the *whitebox* R package which provides an R interface for the WhiteboxTools (Lindsay, 2016).

2.2.4. Land-cover data

Land-cover classification was performed using an automated approach in EnMAP-Box 3 (version 3.11.1, Jakimow et al., 2023) within QGIS. The input raster combined RGB data collected from a SenseFly eBee Classic drone with a Canon IXUS 127 HS 4.3 camera (June–July 2020; 11.4 cm resolution), NDVI, and AGH layers. All layers were resampled to a 1 × 1 m resolution and merged into a single multi-band raster. A training dataset consisting of vector polygons was created for nine land-cover categories: high shrub (generally >1 m, dominated by species such as *Cytisus scoparius, Erica arborea* and *Ulex europaeus*), low shrub (<1 m, primarily *Erica australis, Calluna vulgaris* and *Genista tridentata*), oak forest, pine forest, rock, agriculture, urban, water, and roads. Each category was delineated based on field knowledge and aerial imagery interpretation, with the shrub height threshold chosen to capture both structural differences and distinct species assemblages that are ecologically relevant in the study area. Classification was conducted using the Classic Classification Workflow in EnMAP-Box with a Random Forest classifier (100 trees, 3-fold cross-validation). The model was trained and validated on stratified subsets and final land-cover categories were assigned to each pixel based on majority voting.

2.3. Vegetation sampling design

For the sampling design, the study area was first divided into seven habitat categories based on data derived from 2020 remote sensing imagery: oak forest, pine forest, high shrub, low shrub, rock, agriculture, and others (e.g., urban, roads, waterbodies). Within each suitable habitat type, patches were then further categorized based on the mean NDVI value of the patch to represent variations in vegetation structure and biomass, with four levels based on quartiles: low (0–0.48), medium-low (0.48–0.64), medium-high (0.64–0.74), and high (0.74–0.95). Sampling locations were determined using QGIS, prioritizing accessibility, with at least three locations per habitat/NDVI combination. Where fewer accessible locations were available, we sampled as many as possible.

2.4. Field sampling

In the field, plots were located using a handheld Garmin GPSMAP 64st providing a horizontal position accuracy of ±3.65 m. Sampling was conducted as close to the predefined GPS coordinates as accessibility allowed. At each side, a 20-m transect was established, with the bearing chosen based on optimal representativeness of the surrounding vegetation structure. To account for spatial variability in vegetation cover, four 1 × 1 m subplots were placed every 5 m on alternating sides of the transect (Fig. 1).

Shrub species, which are perennial, evergreen and exhibit only small inter-annual variation in this mostly unmanaged area, were already sampled in September 2023. This data was combined with herbaceous biomass data collected in May 2024. In each subplot, we recorded the percentage cover, average height, and maximum height for each species, but only for individuals up to 2 m. This height threshold reflected the estimated maximum browsing height of the large herbivores in the study area. For shrubs exceeding 2 m, only the biomass within the accessible range was sampled, and any biomass above this height was excluded from analysis. Shrub HAB was collected on a species level, and fresh weight was measured in the field using a scale with 1-g resolution. A subsample of at least 50 g per sample was oven-dried until a stable weight was achieved to determine dry weight.

In May 2024, sampling was repeated in adjacent plots. Percentage cover and height were recorded for the forb and grass layers without species identification. All herbaceous biomass was harvested, sorted into grasses and forbs, weighed and oven-dried separately to determine dry weight per plot. Shrub HAB in May was estimated using species-specific allometric equations derived from the September 2023 data. By recording height and percentage cover of each species in May 2024, we fit allometric equations following Vega et al. (2022) to estimate live shrub HAB for the May 2024 plots (Suppl. Mat. S2).

2.5. Data analysis

For our analysis, we estimated all variables (Table 1) at the plot level by reconstructing the transects and the locations of each sampling plot based on the recorded GPS coordinates and bearing of the transect in QGIS (version 3.38.3). We then calculated the respective values within a squared buffer of 2.5 m in radius surrounding each plot using the Zonal Statistics Tool. To assess relationships between variables, we conducted a Spearman rank correlation test to identify and remove pairs of variables with high correlation coefficients ($\rho > 0.7$). Additionally, we employed a Variance Inflation Factor (VIF) analysis on the remaining variables, where variables with VIF values exceeding a conservative threshold (VIF >5) were excluded from the final models.

2.5.1. HAB estimation model

For the statistical analysis, we employed Generalized Additive Mixed Models (GAMMs) using the *mgcv* package in R (version 4.2.1; R Core

Table 1
Overview of the 19 variables considered in the models, categorized by metric type. Each variable is described along with its corresponding datatype, including topographic, spectral, LiDAR, and land-cover metrics.

Metric	Description	Datatype
Elevation	Mean Elevation [m.a.s.l.] derived from DEMs	Topographic
Slope	Mean Slope [degrees] derived from DEMs	Topographic
Aspect	Mean Aspect [degrees] derived from DEMs	Topographic
NDVI	Mean, Minimum & Maximum of Normalized Difference Vegetation Index	Spectral
CC	Mean, Minimum & Maximum of Canopy Cover [%]	Structural
AGH	Mean, Minimum & Maximum of Aboveground Height [m]	Structural
VRD	Vertical relative point density at certain height intervals (0–0.25m, 0.25–0.5m, 0.5–1m, 1–2m), proportion of returns relative to all returns below 2 m within a pixel [%]	Structural
PH	Percent of vegetation in height ranges (0–0.25m, 0.25–0.5m, 0.5–1m, 1–2m), proportion of returns relative to all returns within that pixel [%]	Structural
LULC	Land-use/Land-cover type obtained through automated Random Forest Classification based on RGB, NDVI & AGH	Land-cover

Team, 2022; Wood, 2011). GAMMs were selected to address several critical aspects of our data and study design such as non-linear relationships between HAB and predictor variables (Li et al., 2017). GAMMs allow for the inclusion of smooth terms, making them well-suited for capturing complex, non-linear patterns. Additionally, the hierarchical structure of our data, with plots nested within transects, introduced non-independence among plots. To account for spatial autocorrelation, we included transect ID as a random effect, thereby allowing for plot-level variation while controlling for transect-level dependencies. To verify whether this adequately removed spatial autocorrelation, we later tested the model residuals for spatial dependence using Moran's I, calculated across a range of neighborhood sizes (k-nearest neighbors with k = 1–15). Moran's I values close to zero indicate that residuals are spatially independent, confirming that spatial autocorrelation was effectively accounted for in the fitted model.

Because the continuous response variable (HAB) exhibited an excess of zeros, we used a Tweedie distribution, which accommodates zero-inflated continuous data with non-negative support without requiring a separate zero-inflation model. This approach provided a robust and flexible framework for analyzing HAB data across shrub, forb, grass, total and combined herbaceous HAB categories.

While our study aimed at estimating HAB below 2 m, we did not disregard remote sensing information from vegetation exceeding this height. Structural and spectral signals above 2 m, such as AGH or NDVI, can still provide important ecological context, particularly in relation to light availability and competitive pressure on the understory. For instance, high NDVI values may indicate dense tree canopy and low understory biomass in forested areas, whereas in shrublands, similar NDVI values typically reflect accessible shrub biomass. To capture these context-dependent relationships, we included land-cover type (LULC) as a predictor and modeled interactions between LULC and both NDVI and AGH. This approach allowed us to account for differing relationships between remote sensing signals and understory HAB across habitat types, improving our ability to estimate HAB.

We applied smoothing functions to all continuous variables to enhance model flexibility, and used a circular smooth for Aspect to appropriately address its circular nature. Models were fitted using restricted maximum likelihood (REML), with diagnostic plots used to assess homoscedasticity and normality of residuals. To enable effective variable selection, we employed a double penalty approach (also referred to as *null space penalization*) as described by Marra and Wood (2011). This method introduces an additional penalty targeting the null space of a smooth term's penalty matrix, such as linear trends in splines. This allows the model to completely remove non-contributory smooth terms, achieving effective variable selection (Marra and Wood, 2011). In the *mgcv* package, this is implemented by setting *select* = *TRUE* in the *gam* function.

2.5.2. Cross-validation procedure for model evaluation

Model performance was first evaluated using the deviance explained metric from the model summary, which quantifies the proportion of total variation in the response variable that is accounted for by the model, based on a comparison between the residual deviance of the fitted model and the null deviance from an intercept-only model. To assess predictive ability of the model while limiting risk of overfitting, we implemented a repeated Monte Carlo cross-validation procedure. In each iteration, the dataset was randomly split into 80 % training and 20 % validation subsets. Splitting was stratified by habitat type and constrained at the transect level to ensure all habitat types were represented in each subset and to prevent spatial information leakage between transects. The model was then refitted to the training data, and predictions were generated for the validation data. This procedure was repeated 1000 times, generating distributions of model performance metrics to assess both mean predictive ability and its variability across resamples. In addition, the penalization of smooth terms (select = TRUE) reduced the influence of non-contributing predictors and limited model complexity. Together, these measures reduce the risk of overfitting and provide a conservative estimate of predictive ability within the sampled landscape. We note however, that without truly independent external data, some residual risk of overfitting remains.

2.5.3. Variable effects and HAB prediction

Unlike traditional regression, generalized additive models use smooth functions to capture complex, nonlinear relationships, rather than producing easily interpreted coefficients. Following this, we assessed variable importance using F-statistics extracted from the model summaries and visualized predictor effects on HAB using the *visreg* function from the *visreg* package in R (Breheny and Burchett, 2017), which plot the partial effect of a predictor while holding other predictors constant.

To predict HAB across the entire study area we created a 10 × 10 m resolution grid covering the full extent of the study area in QGIS. All covariates used in the modelling procedure were then extracted for each grid cell using the Zonal Statistics Tool. The resulting grid-level dataset was exported from QGIS and imported into R, where HAB predictions were generated using the *predict.gam* function from the *mgcv* package. In addition to predicted HAB values, we extracted the associated standard errors of the predictions. These were used to calculate the coefficient of variation (CV) for each grid cell, providing a spatial estimate of prediction uncertainty. All resulting maps, including HAB and uncertainty layers, were produced using QGIS.

3. Results

Herbivore-accessible biomass (HAB) varied strongly across habitats, with the highest values in shrublands and agricultural pastures and the lowest in oak and pine forests. Models showed that topographic, structural, and spectral variables significantly influenced biomass patterns, with effects differing by vegetation type and habitat. Total and shrub HAB models performed well overall, though predictions in high-biomass areas were often underestimated and herbaceous components showed greater variability and uncertainty. Spatial predictions revealed strong habitat-driven patterns, with shrubs contributing the majority of biomass, and herbaceous biomass most abundant in agricultural areas.

3.1. Field summary

In total, we sampled 48 transects across six habitat categories, resulting in data from 192 plots for the analysis. The mean elevation was 956 m, ranging from 806 to 1,198 m, thereby covering nearly the entire elevation gradient of the study area (mean = 1038 m, min = 745 m, max = 1,267 m). The average slope of the plots was 16.17°, with a range from 0.93° to 49.24°. Although the slope within the study area varies from 0° to 70.99°, it was not feasible to sample plots with slopes greater than 50°. The average NDVI of the plots was 0.64 ± 0.19, with the highest values observed in oak forests (0.85 ± 0.07) and agricultural patches (0.84 ± 0.07), and the lowest in low shrub habitats (0.52 ± 0.20) and rocky outcrops (0.54 ± 0.12).

The mean total plant cover varied notably across habitats, with the highest values in agricultural pastures and the lowest in pine forests (Table 2). Shrub cover was most extensive in high shrub habitats and sparse in oak forests. Forb and grass cover peaked in agricultural pastures and oak forests, while being relatively low in other habitat types. Total HAB was highest in high shrub habitats, followed by low shrub habitats, and lowest in oak forests (Table 2, Fig. S5). Shrub HAB followed a similar pattern, with high shrub habitats supporting the greatest HAB, and oak forests and agricultural areas the least. In contrast, agricultural pastures exhibited the highest forb HAB, while rocky outcrops showed the lowest. Similarly, grass HAB was highest in agricultural pastures and low shrub habitats, with significantly lower values observed in rocky areas. Across all metrics, the variation between plots was high, as shown by the high standard deviations, especially in forest

Table 2
Field measurements of herbivore-accessible HAB (HAB) and cover across different habitat types, presented as mean ± standard deviation (SD). Variables include total cover, total HAB, shrub cover and HAB, forb cover and HAB, and grass cover and HAB.

	Total cover [%]	Total HAB [g/m^2]	Shrub cover [%]	Shrub HAB [g/m^2]	Forb cover [%]	Forb HAB [g/m^2]	Grass cover [%]	Grass HAB [g/m^2]
Agriculture	83.36 ± 12.19	132.88 ± 45.60	6.29 ± 8.45	32.22 ± 44.59	43.57 ± 18.65	44.25 ± 22.42	45.71 ± 18.07	56.41 ± 31.41
High Shrub	59.53 ± 26.78	310.86 ± 265.60	36.50 ± 26.74	276.84 ± 258.21	5.75 ± 6.77	4.86 ± 5.54	28.88 ± 29.85	29.16 ± 47.09
Low Shrub	69.17 ± 17.22	249.95 ± 146.05	44.18 ± 29.07	198.50 ± 153.40	5.78 ± 7.74	7.12 ± 9.79	27.24 ± 20.61	44.33 ± 47.46
Oak Forest	44.97 ± 26.63	63.23 ± 164.63	7.52 ± 18.92	42.62 ± 149.41	8.49 ± 12.69	4.76 ± 10.26	33.22 ± 27.81	12.68 ± 17.91
Pine Forest	43.13 ± 24.64	123.65 ± 136.90	20.48 ± 22.88	98.85 ± 134.39	10.76 ± 11.16	9.84 ± 13.09	16.02 ± 13.37	10.24 ± 11.14
Rock	52.80 ± 23.87	204.51 ± 144.70	42.48 ± 28.22	191.28 ± 148.26	4.81 ± 7.65	4.05 ± 10.39	8.85 ± 15.35	9.18 ± 13.25
Total	**56.73 ± 25.66**	**191.41 ± 184.79**	**30.64 ± 29.10**	**157.01 ± 183.08**	**9.34 ± 14.05**	**8.51 ± 15.18**	**23.18 ± 24.12**	**23.14 ± 34.78**

habitats. Average shrub height was 39.94 cm (IQR = 8.25–51.50 cm; Fig. S2), with highest values in high shrub habitats (mean = 87.70 cm). Forbs grew on average 11.22 cm tall (IQR = 4–14 cm), with consistent heights across habitat types, while grasses were slightly taller (mean = 14.69 cm; IQR = 8–19 cm; Fig. S2).

3.2. Automated land-cover classification

The automated land-cover classification achieved an overall accuracy of 73.08 % [95 % CI: 73.0–73.13 %], with the highest Producer's Accuracy in oak forests (87.74 %) and rocky habitats (88.34 %). Accuracies were lowest for shrubland habitats, with 35.09 % for high shrub and 42.86 % for low shrub (Table S1.2 and S1.3), largely due to frequent misclassification between those two categories (Table S1.1). Similarly, the model struggled to separate pine forests from oak forests and occasionally misclassified urban areas as rocky habitats. Despite these limitations, the model performed significantly better than random, as indicated by the Kappa Accuracy of 65.59 % (Table S1.2).

To address the high misclassification between rocky outcrops and urban areas, we manually created a reference raster file delineating the

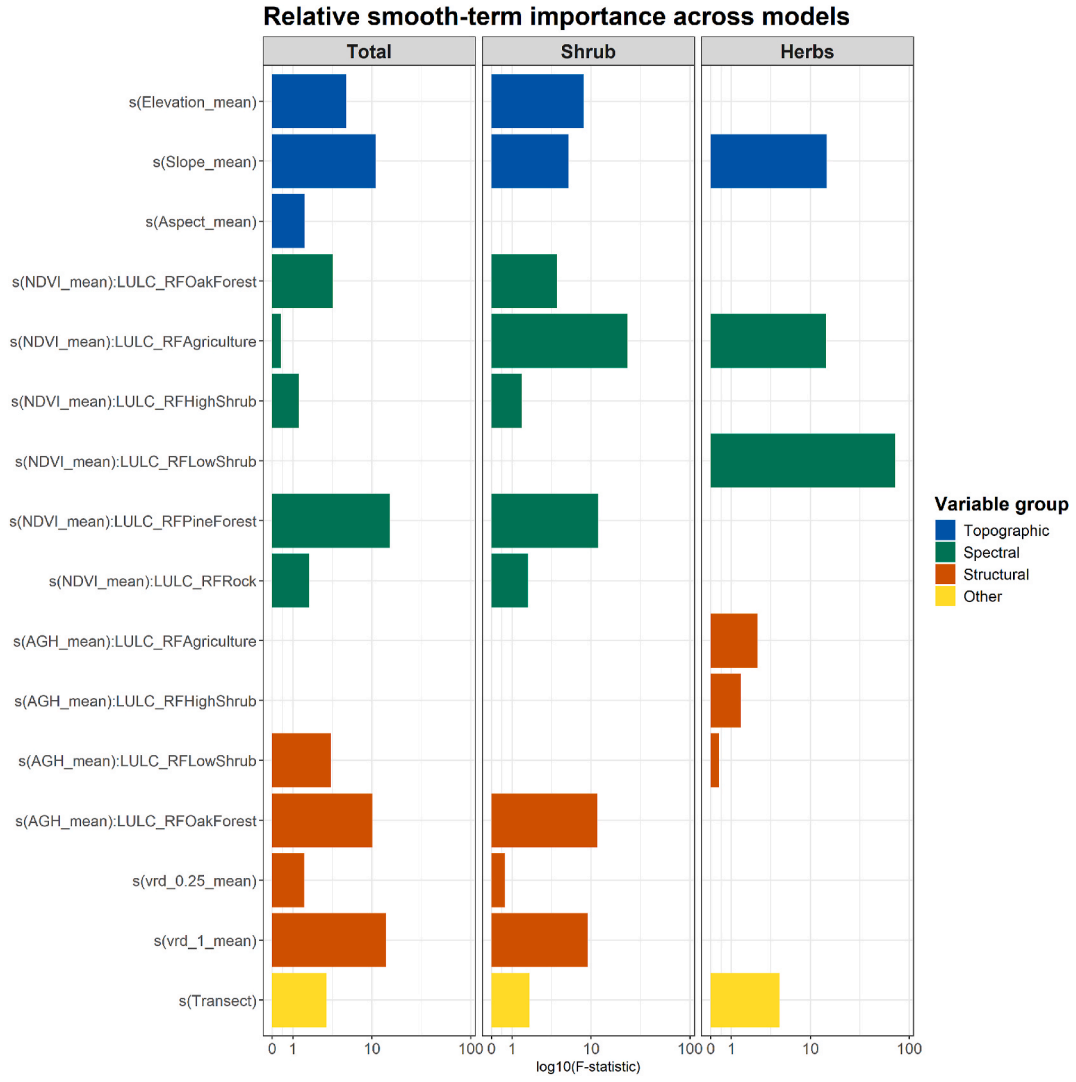

Fig. 2. Relative importance of smooth terms expressed as F-statistics from generalized additive models predicting total, shrub and herbaceous HAB. The y-axis is presented on a log10 scale to show the range of values. Terms with negligible importance ($F \leq 0.001$ across all models) were excluded to improve clarity. Variables are grouped by data type including topographic, spectral, structural, and other categories and colored accordingly. Results for forb and grass HAB models are provided separately in the supplementary materials.

study area into urban/roads and natural land-covers. Based on this raster, misclassified pixels were corrected by reassigning any urban/road pixels outside urban zones to rock, and any non-urban classifications within urban zones to urban/road. To further reduce classification noise and correct small misclassifications, a smoothing filter was applied using the *r.neighbors* function from the GRASS plugin in QGIS, with a circular 9 x 9 neighborhood assigning each pixel the most frequent class within its vicinity.

3.3. Variable selection and importance

After checking for correlation and multicollinearity (Supplemental Material S5.1 to S5.3), the following variables were retained for modeling: LULC, Elevation, Slope, Aspect, NDVI_mean, AGH_mean, CC_min, vrd_0, vrd_0.25, vrd_0.5, and vrd_1. PH had to be removed due to high correlation (>0.7) with VRD as well as AGH and CC.

When comparing HAB across habitat types, shrub HAB was highest in high shrub areas and lowest in oak forests, aligning with expected vegetation structure. Herbaceous HAB was significantly higher in agricultural patches than in all other habitat types. Forbs were generally lower in high shrub, low shrub, oak, and pine forests, while rocky habitats showed no significant difference. Grass HAB was significantly reduced in oak and pine forests, and marginally lower in high and low shrub habitats.

Across models, HAB distribution was influenced by a range of topographic, spectral, and structural variables, with variable effects depending on vegetation type and habitat context. Elevation consistently showed a negative relationship with both total and shrub HAB (total: edf = 0.63, F = 5.33, p = 0.09; shrub: edf = 0.77, F = 8.37, p = 0.04; Fig. 2), although it was excluded from the forb, grass, and herbaceous models due to increased prediction errors. Slope also negatively affected HAB across models, significantly influencing total (edf = 1.11, F = 10.99, p = 0.01), shrub (edf = 0.82, F = 5.80, p = 0.02), and herbaceous HAB (edf = 0.80, F = 14.67, p = 0.03; Fig. 2). Aspect was only significant in the individual forb and grass models, where southeast-facing slopes appeared weakly associated with increased HAB (see Model Summaries S7 in the Supplemental Material).

NDVI emerged as an important spectral predictor, although its effects were habitat-dependent. In forest habitats, higher NDVI values were significantly associated with reduced total and shrub HAB, for example in oak forests (total: edf = 0.87, F = 3.80, p = 0.00; shrub: edf = 0.90, F = 4.37, p = 0.00) and pine forests (total: edf = 0.90, F = 11.79, p = 0.00; Fig. 2). A similar negative NDVI effect was observed for herbaceous HAB in low shrub habitats (edf = 0.73, F = 28.35, p = 0.06), and for shrub HAB in agricultural areas (edf = 1.75, F = 23.37, p = 0.00; Fig. 2). Aboveground height (AGH) also exhibited variable effects by habitat and biomass type. Notably, AGH negatively affected total and shrub HAB in oak forests (total: edf = 1.66, F = 10.04, p = 0.00; shrub: edf = 0.96, F = 11.56, p = 0.00, Fig. 2). These patterns suggest that taller vegetation is linked to reduced understory productivity in forest habitats. LiDAR-derived vertical return density (vrd) metrics contributed meaningfully to the models, particularly for total and shrub HAB. Higher return densities between 0.25 and 0.50 m (total: edf = 0.89, F = 1.63, p = 0.08), as well as between 1 and 2 m (total: edf = 1.57, F = 13.85, p = 0.01; shrub: edf = 1.41, F = 9.23, p = 0.02) were associated with increased HAB, reflecting denser vegetation at relevant height classes (Fig. 2).

Overall, the models underscore the importance of topographic, structural, and spectral variables in shaping biomass patterns across Mediterranean landscapes. Topographic features such as elevation and slope were consistently important across vegetation strata, particularly for total and shrub HAB (Fig. 2). Spectral information, especially NDVI, played a central role in predicting herbaceous HAB, while both spectral and structural metrics (e.g., vertical return densities and AGH) were key predictors for total and shrub HAB (Fig. 2).

3.4. Model performance

The total HAB model demonstrated notable explanatory power, accounting for a substantial portion of biomass variability across plots (pseudo $R^2 = 0.64$, Deviance Explained = 0.77; Table 3). Incorporating Transect as a random effect (edf = 34.54, F = 3.22, p < 0.00) successfully accounted for spatial autocorrelation. Moran's I values of the residuals were consistently close to zero and slightly negative (ranging from −0.23 to −0.04 across k, Table S9), indicating no evidence of positive spatial autocorrelation. The random effect captured substantial site-level variability and enhanced model fit, indicating a high degree of spatial variability between plots that is not fully explained by the environmental predictors alone. This is also reflected in the cross-validation statistics, where the model demonstrated only moderate predictive performance on unseen data when transect was excluded ($R^2_{80} = 0.34$, $RMSE_{80} = 160.28$ g/m^2, $R^2_{20} = 0.20$, $RMSE_{20} = 172.38$ g/m^2; Fig. 3, Table 3), with the high RMSE largely driven by a few high-biomass plots. The model slightly underestimated HAB, with an average bias of −39.08 g/m^2 in the training set and −32.58 g/m^2 in the validation set, primarily due to underestimation in very high biomass patches (Fig. 3, Table 3).

The shrub HAB model also explained a significant proportion of variance (pseudo $R^2 = 0.62$, Deviance Explained = 0.77; Table 3). Cross-validation metrics were comparable to those of the total HAB model, although it performed less well on the validation data, with $R^2_{80} = 0.38$, $RMSE_{80} = 153.70$ g/m^2, $R^2_{20} = 0.24$, $RMSE_{20} = 410.21$ g/m^2 and a very small bias of 2.97 g/m^2 in the validation dataset (Fig. 3, Table 3). However, performance of the shrub model was slightly better in extremely low and high biomass patches. In contrast, the forb HAB model accounted for a substantial proportion of variance (pseudo R^2 = 0.77, Deviance Explained = 0.78), while cross-validation highlighted some challenges in predictive accuracy ($R^2_{80} = 0.49$, $RMSE_{80} = 11.75$ g/m^2, $R^2_{20} = 0.35$, $RSME_{20} = 12.36$ g/m^2). It also exhibited a consistent negative prediction bias of −3.93 g/m^2 in the validation data (Table 3, Fig. S10). The grass HAB model demonstrated slightly lower explanatory power (pseudo R^2 = 0.63, Deviance Explained = 0.65) and cross-validation results indicated low predictive performance (R^2_{80} = 0.30, $RMSE_{80}$ = 31.09 g/m^2, R^2_{20} = 0.24, $RSME_{20}$ = 29.78 g/m^2; Table 3, Fig. S10). However, while the model seemed to overestimate HAB slightly in very low biomass areas, on average it underestimated HAB, showing a bias of −8.61 g/m^2 on unseen data (Table 3). In comparison, the herbaceous HAB model explained a higher proportion of variance (pseudo $R^2 = 0.68$, Deviance Explained = 0.69), while cross-validation also revealed a slight increase in predictive performance (R^2_{80} = 0.40, $RMSE_{80}$ = 34.43 g/m^2, R^2_{20} = 0.34, $RMSE_{20}$ = 34.25 g/m^2; Fig. 3, Table 3). Once more, we observed a consistent negative bias of −10.90 g/m^2, mostly in areas of very high herbaceous biomass (Fig. 3, Table 3).

3.5. HAB predictions

The total HAB model effectively predicted HAB across the study area, with a mean estimate of 130.77 ± 55.64 g/m^2, revealing clear spatial

Table 3
Model summary and cross-validation metrics for each vegetation type including R^2, deviance explained, RMSE, Bias, and R^2 for training (80) and validation (20) datasets.

	Total	Shrub	Forb	Grass	Herb
R^2	0.64	0.62	0.77	0.63	0.68
Dev.Exp	0.77	0.71	0.78	0.65	0.69
$RMSE_{80}$	160.28	153.70	11.75	31.09	34.43
$RMSE_{20}$	172.38	410.21	12.36	29.78	34.25
$Bias_{80}$	−39.08	−37.05	−3.94	−8.56	−10.64
$Bias_{20}$	−32.58	2.97	−3.93	−8.61	−10.90
R^2_{80}	0.34	0.38	0.49	0.30	0.40
R^2_{20}	0.20	0.24	0.35	0.24	0.34

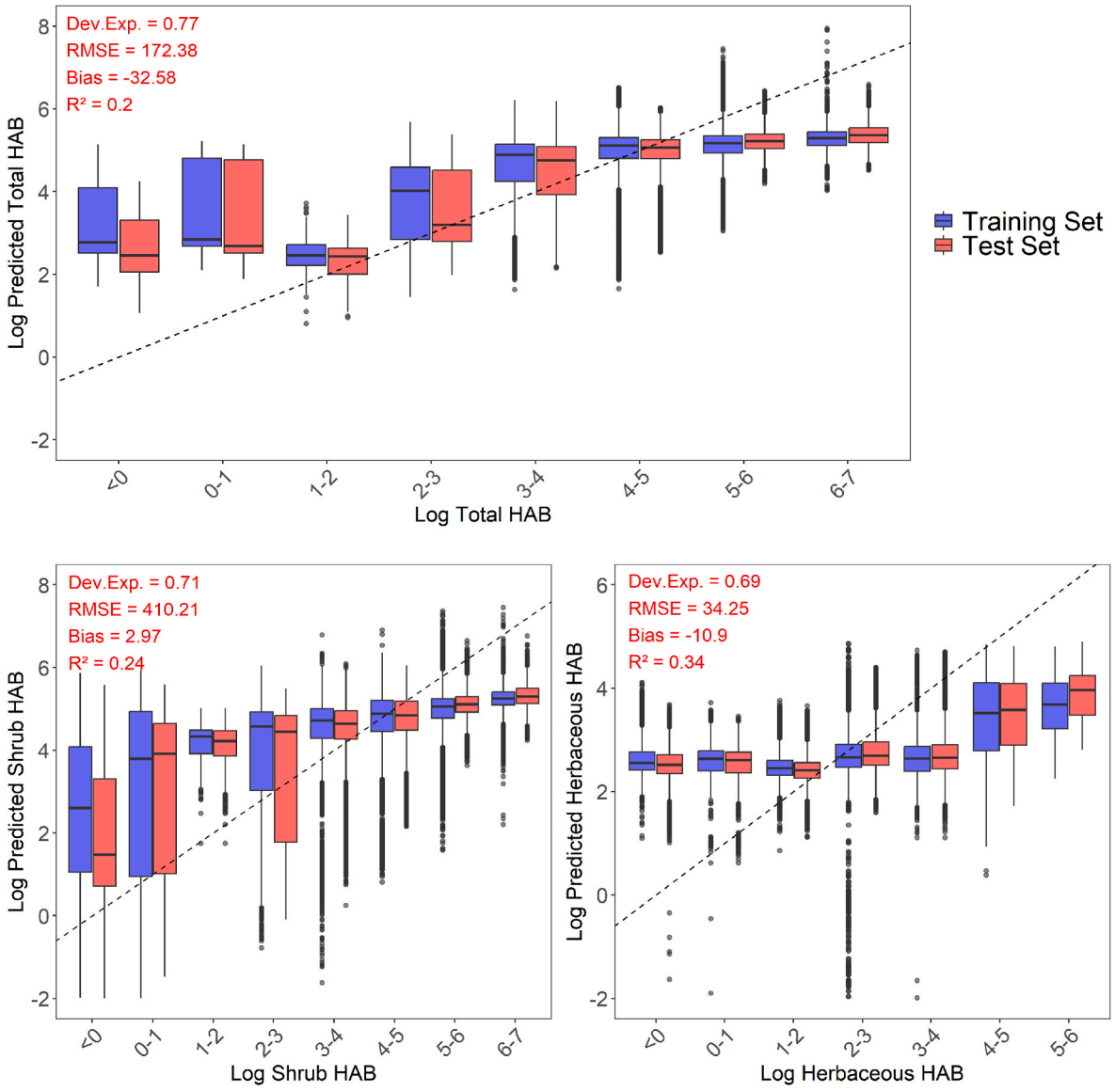

Fig. 3. Predicted vs. observed HAB across total HAB (top), shrub HAB (bottom left), and herbaceous HAB (bottom right) using hold-out cross-validation. Predictions were generated using an 80/20 training-validation split at both the habitat and transect levels, ensuring data independence. The blue and red boxplots represent the log HAB predictions of the training and test sets, respectively. The dashed 1:1 line represents perfect agreement between predicted and observed values. Key performance metrics, including deviance explained (Dev.Exp), root mean square error (RMSE), bias, and R^2 are provided for the 20 % validation dataset.

patterns consistent with habitat distribution (Table S10). HAB was highest in shrub habitats (183.24 ± 33.86 g/m^2 in low shrubs) predominantly located at intermediate elevation and slope levels (Fig. 4, Table S10, Figure S13.1). Conversely, oak forests in the valleys exhibited the lowest HAB estimates (85.47 ± 61.71 g/m^2), reflecting low understory vegetation (Fig. 4, Table S10, Figure S13.1). Although the model performed well in lower biomass habitats, it underestimated HAB in high-density shrublands compared to field data. Mean field measurements ranged from 63.23 ± 164.63 g/m^2 in oak forests to 310.86 ± 265.6 g/m^2 in high shrub habitats (Table S10). The larger standard deviations in the field data indicate that the model fails to capture the full variability observed, particularly at the extremes of the biomass spectrum. This suggests limited sensitivity to complex environmental gradients or biotic factors influencing high biomass zones. Despite this, the coefficient of variation (CV) of the predictions was considerably low at 27.08 ± 7.08 %, with the highest values in oak forests (34.05 ± 5.29 %) and the lowest in low shrub habitats (21.72 ± 3.73 %, Fig. 4, Figure S13.2). This pattern reflects greater prediction confidence in high-biomass areas and increased uncertainty in more heterogeneous, low-biomass habitats.

The shrub HAB predictions followed a similar pattern. Average shrub HAB was estimated at 102.81 ± 76.35 g/m^2, with the lowest HAB in pine forests (68.27 ± 46.27 g/m^2) and oak forests (71.24 ± 69.63 g/m^2), and the highest in high shrub habitats (142.11 ± 50.51 g/m^2; Fig. 4, Table S10, Figure S13.1). As with total HAB, the model tended to underestimate shrub HAB in high-density areas but performed reasonably well in forested habitats. However, the model's limited ability to capture the full variability in shrub HAB is reflected by the differences in standard deviations between actual and predicted values (Table S10). Prediction uncertainty was notably higher in agricultural areas (62.74 ± 20.06 %) and forests (39.39 ± 7.78 % in oak forests and 35.11 ± 10.69 % in pine forests), leading to a higher general CV of 32.53 ± 10.16 % (Fig. 4, Figure S13.2).

Forb and grass HAB predictions exhibited higher uncertainty. Mean predicted forb HAB was at 3.42 ± 3.27 g/m^2 (Figs. S10 and S11), much lower than field estimates (8.51 ± 15.18 g/m^2; Table S11). Grass HAB predictions averaged 9.96 ± 6.54 g/m^2 (Fig. S12, Table S11), also below field data (23.14 ± 34.78 g/m^2). This disparity suggests the model did

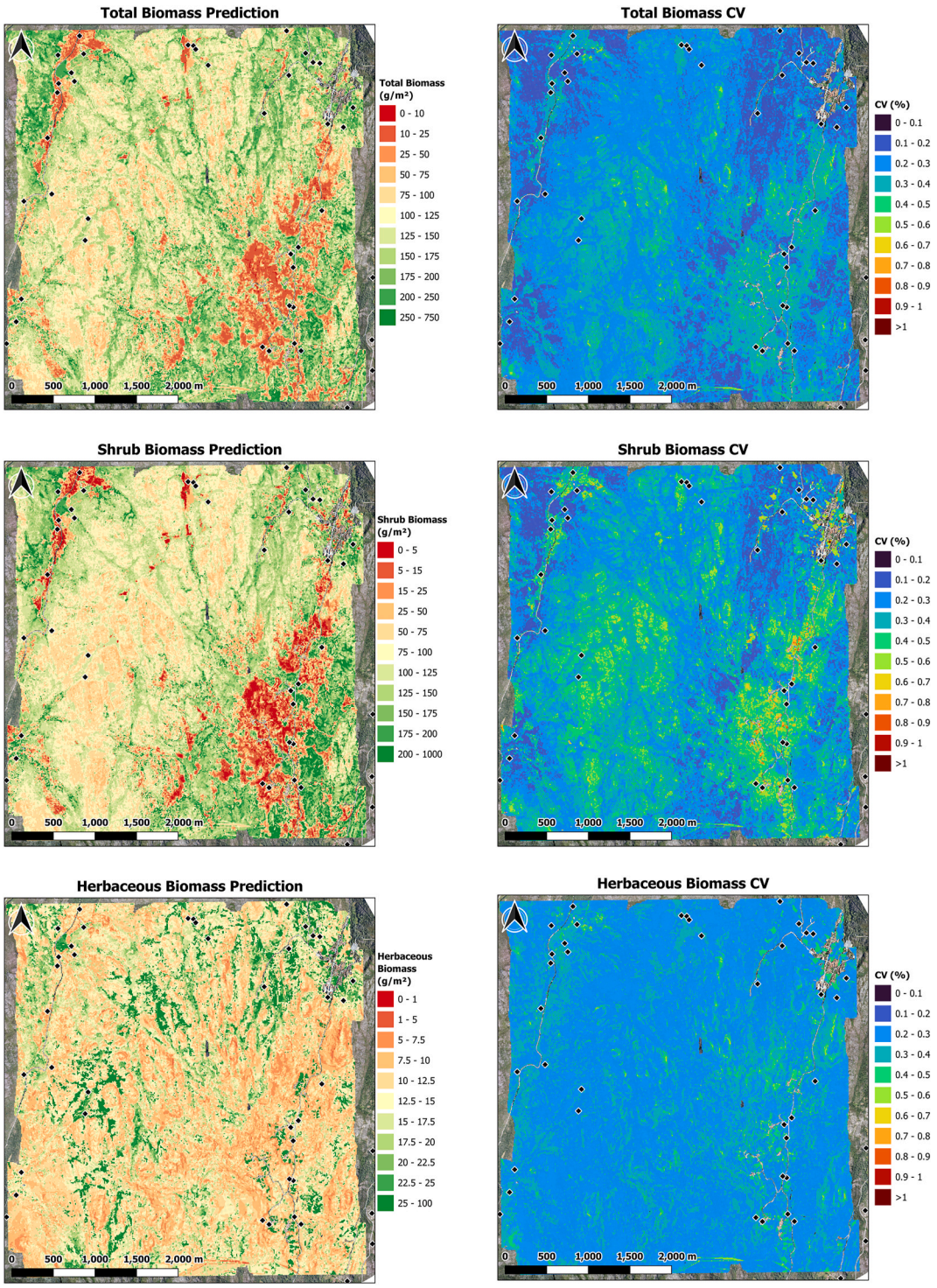

Fig. 4. HAB predictions across the study area, displayed on a 10 × 10m grid: (Top) Total HAB, (Middle) Shrub HAB, and (Bottom) Herbaceous HAB. Predictions (g/m^2) are shown on the left, with the coefficient of variation (CV), representing the uncertainty of the predictions, shown on the right. CV is calculated from the standard error of the predictions obtained via the predict function (se.fit = T). The spatial extent of the grid covers approximately 18 ha, providing a fine-scale representation of HAB distribution across the study area.

not adequately capture the patchy and highly variable distribution in the field, and that environmental variables alone could not explain the variability between transects, leading to predictions that primarily reflect averages. Especially the forb predictions inhibited a high CVs (57.62 ± 21.32 %; compared to 33.53 ± 5.34 % in the grass predictions) across most land-cover types, highlighting the extremely high variability in the herbaceous layer, likely influenced by local disturbances and land use practices (Fig. S12).

Given this, we focused on the combined herbaceous HAB model for forbs and grasses. The predicted herbaceous HAB averaged 14.33 ± 8.34 g/m^2, which was still notably lower than field measurements of 31.93 ± 41.31 g/m^2 (Table S11, Figure S13.1). Agricultural pastures had the highest predicted HAB (67.92 ± 13.23 g/m^2), though still lower than field data (100.66 ± 41.31 g/m^2). Predictions were lowest in oak

forests (10.35 ± 2.27 g/m^2), pine forests (11.68 ± 2.62 g/m^2), and rocky outcrops (11.49 ± 2.36 g/m^2), aligning more closely with field data (Table S11). Additionally, herbaceous HAB showed a strong correlation with slope, with areas with slopes above approximately 35° only exhibiting little to no herbaceous plants (Fig. 4). Nevertheless, the herbaceous HAB model showed improved prediction certainty compared to the individual models, with a mean CV of 28.75 ± 4.78 %, lowest in rocky habitats (26.43 ± 4.03 %) and highest in agricultural patches (45.10 ± 1.87 %; Fig. 4, Table S11, Figure S13.2).

Overall, total HAB across the entire study area was estimated at 2,369 tons, averaging 1.31 tons/ha (Table 4). Shrubs represented the largest HAB component, contributing 1,862 tons, or 1.02 tons/ha. In comparison, forbs and grasses accounted for approximately 62 tons and 180 tons, respectively, while the herbaceous model predicted HAB across the entire study area at 259 tons, or 0.14 tons/ha (Table 4). High shrub areas exhibited the highest total HAB density, reaching 1.83 tons/ha, while forested areas had the lowest HAB, with oak forests at 0.85 tons/ha and pine forests at 0.94 tons/ha (Table 4). Shrub HAB was most prevalent in high shrub habitats (1.42 tons/ha), while agricultural pastures were characterized by a higher proportion of herbaceous HAB (0.68 tons/ha) and lower shrub HAB (1.00 tons/ha). These patterns in HAB distribution reflect the expected ecological characteristics of different habitat types across the study area.

4. Discussion

This study used high-resolution UAV-derived remote sensing data to model herbivore-accessible biomass (HAB) across a structurally and ecologically diverse landscape. By incorporating land cover type into the modeling framework, we predicted HAB across multiple vegetation types without separate models. These are the first estimates of shrub and herbaceous HAB in the Peneda-Gerês National Park, offering valuable insights into ecosystem structure, while establishing a baseline to support future research on the ecological impacts of rural depopulation and land abandonment. HAB and plant cover varied across habitat types, with agricultural pastures showing the highest herbaceous HAB, while shrub habitats supported the greatest total and shrub HAB. Key environmental variables such as elevation, slope, NDVI, and LiDAR-derived structural metrics, significantly influenced HAB distribution, though their effects differed across vegetation strata and habitats.

Unlike conventional biomass assessments aimed at carbon stocks or fuel load assessments across all vegetation layers (Aranha et al., 2020; Casals et al., 2023; Pasalodos-Tato et al., 2015; Vega et al., 2022), this study focused on live biomass below 2 m, a critical and understudied resource for herbivores. Our results highlight the value of high-resolution remote sensing data to model this type of biomass at a landscape scale, making a valuable step toward understanding herbivore-resource dynamics. Nonetheless, the high heterogeneity in HAB across the study area underscores the importance of accounting for spatial heterogeneity in both field measurements and model interpretation.

4.1. Variable selection and habitat-dependent effects on HAB

We reduced multicollinearity using a two-step approach: first removing strongly correlated variables based on Spearman's ρ, followed by VIF analysis to identify remaining redundancy. While this is a common and interpretable method in GAM-based ecological models, it involves some subjectivity in threshold selection. More systematic alternatives (e.g., PCA or regularization) may address collinearity differently but can limit interpretability, which was a key consideration in this study.

To address the high variability in our field data and account for spatial autocorrelation, we incorporated Transect as a random effect in our models, which explained a substantial portion of the deviance. We chose not to include a spatial smoothing term (s(Lat, Lon)) because the pronounced environmental heterogeneity and habitat patchiness in our study area could have caused such a term to obscure the effects of key spatial predictors like elevation and land use, reducing interpretability of individual variable contributions. This random effect structure effectively addressed spatial autocorrelation, as confirmed by Moran's I values of the model residuals, which were consistently close to zero and slightly negative across a range of neighborhood sizes. This indicates that spatial dependence among plots was adequately accounted for by the transect-level random effect, supporting the suitability of our modeling approach for disentangling the influence of individual environmental predictors. Although NDVI data were collected in May 2023 and LiDAR metrics in May 2024 together with the field sampling campaign, inter-annual variability in vegetation biomass in the study area is low, and there were no major disturbances such as fires. Therefore, the temporal mismatch between datasets is unlikely to have affected the observed habitat–biomass relationships.

We found that topographic factors generally showed negative relationships with HAB: higher elevations and steeper slopes tended to be associated with lower HAB, as reported in previous studies (e.g., Wang et al., 2007), while slope also negatively affected herbaceous HAB.

The relationship between NDVI and HAB varied across habitats. In forests, NDVI was negatively correlated with total and shrub HAB, likely because dense canopy cover limits understory growth. Similarly, in agricultural areas, NDVI negatively correlated with shrub HAB, as higher NDVI values reflected herbaceous vegetation that has higher leaf area and chlorophyll content, and typically replaces shrubs after disturbances such as grazing. Conversely, in shrublands and rocky outcrops, NDVI was positively correlated with HAB. These patterns reflect habitat-specific factors such as vegetation structure, light availability, and productivity. For example, high NDVI in forests reflects canopy cover that limits understory growth, whereas in open habitats high NDVI often indicates greater biomass below 2 m. Although NDVI is a widely used biomass proxy (Aranha et al., 2020; Estornell et al., 2012; Greaves et al., 2016), its accuracy is limited in forests due to saturation and its focus on canopy cover, making it less sensitive to understory vegetation (Bazzo et al., 2023; Greaves et al., 2016). Complementary indices, such as EVI, SAVI or GNDVI, may better capture variations in understory and improve predictions in dense vegetation (Bazzo et al., 2023; Riquelme et al., 2022).

In addition, aboveground height, particularly in interaction with

Table 4
HAB density predictions for the entire study area and per habitat type, presented as mean ± standard deviation (SD) in tons per hectare (tons/ha). The table includes total HAB density and HAB densities for specific categories: shrubs, forbs, grasses, and herbs, across different habitat types.

	Area [ha]	Total [tons/ha]	Shrubs [tons/ha]	Forbs [tons/ha]	Grasses [tons/ha]	Herbs [tons/ha]
Agriculture	22.7	1.64 ± 7.94	1.00 ± 13.19	0.23 ± 3.27	0.39 ± 3.96	0.68 ± 6.43
High Shrub	228.66	1.70 ± 2.84	1.42 ± 2.87	0.05 ± 0.15	0.12 ± 0.25	0.16 ± 0.30
Low Shrub	269.85	1.83 ± 2.42	1.33 ± 1.89	0.04 ± 0.12	0.19 ± 0.41	0.24 ± 0.44
Oak Forest	429.5	0.85 ± 1.40	0.71 ± 1.35	0.02 ± 0.05	0.07 ± 0.11	0.10 ± 0.15
Pine Forest	48.59	0.94 ± 3.86	0.66 ± 3.43	0.02 ± 0.16	0.07 ± 0.41	0.12 ± 0.61
Rock	812.19	1.27 ± 1.15	1.01 ± 1.11	0.03 ± 0.07	0.08 ± 0.08	0.11 ± 0.11
Total	**1811.49**	**1.31 ± 0.83**	**1.02 ± 0.0.79**	**0.03 ± 0.05**	**0.10 ± 0.08**	**0.14 ± 0.10**

habitat type, emerged as a key predictor of HAB. In oak forests, maximum AGH negatively affected total and shrub HAB, potentially due to canopy closure limiting light availability, or tall trees limiting water and nutrient availability for understory vegetation. This highlights the importance of considering AGH at various, habitat-dependent levels. Other studies also emphasize the predictive value of canopy height models for biomass estimation. For example, Zhang et al. (2018) identified mean canopy height as the strongest predictor of grassland AGB, though Estornell et al. (2012) caution that LiDAR may underestimate shrub height, potentially impacting biomass predictions in shrub-dominated habitats. Other LiDAR-derived metrics, particularly vertical point densities within specific height intervals, were also important predictors across HAB types, emphasizing the role of vegetation structure, especially shrub density, in biomass prediction. This supports findings from previous studies (Estornell et al., 2012), which identified height-specific point distributions as key for predicting shrub biomass.

4.2. Model accuracy and predictive strength

Predictive performance across all models was considerably strong, with the total HAB and shrub HAB models explaining 77 % and 71 % of the deviance, respectively. These results are comparable to those from more homogeneous habitats. For example, Li et al. (2017) reported R^2 values of 0.74–0.80 for total biomass, and 0.76–0.84 for shrub biomass, depending on modeling algorithm. Estornell et al. (2012) achieved an R^2 of 0.34 using spectral data, 0.67 with LiDAR data, and 0.79 when combining both. Similarly, Greaves et al. (2016) modeled Arctic tundra shrub biomass with R^2 values ranging from 0.60 using LiDAR-derived canopy volume alone to 0.71 when incorporating spectral data.

However, a large portion of this predictive power was due to the inclusion of Transect as a random effect, which captured much of the variability in the data. This combined with the complexity of GAMMs, likely explains the moderate cross-validation performance across models and the similarity between training and validation data. Excluding Transect in the prediction phase limited our ability to capture field-level heterogeneity. As a result, our models tended to underpredict in high biomass areas across almost all habitat and vegetation classes. Additionally, the low standard deviations of the predictions compared to actual HAB values, indicate a tendency to smooth out high variability, leading to predictions that reflect averages rather than capturing the full HAB range. The environmental predictors alone were insufficient to explain fine-scale differences. Capturing extreme values therefore remains a challenge in heterogeneous landscapes.

Our models achieved $RMSE_{20}$ values of 172.38 g/m^2 for total and 410.21 g/m^2 for shrub HAB, similar to some studies, such as Li et al. (2017), which found RMSE values of 141 g/m^2 for total biomass and 152 g/m^2 for shrub biomass, or Greaves et al. (2016), with RMSE values from 197.0 g/m^2 to 239.5 g/m^2. However, RMSE is highly context-dependent, varying with study area, biomass range and methods, making direct comparisons unreliable. For example, Estornell et al. (2012), reported much higher RMSE (966 g/m^2) despite achieving similar R^2 values. Since we focused on herbivore-accessible biomass, comparing our results to studies estimating total biomass, including woody components of shrubs, is not valid.

For herbaceous HAB, comparisons with other studies remain valid since we estimated total herbaceous biomass, which did not exceed 2 m. The combined herbaceous model showed moderate performance (Deviance Explained = 0.69, $RMSE_{20}$ = 34.25 g/m^2) with values slightly below other remote sensing based models for grass or herbaceous biomass. For example, Lussem et al. (2019) achieved R^2 values between 0.78 and 0.87 with RMSE ranging from 27.4 to 41.6 g/m^2, while Zhang et al. (2018) reported an R^2 of 0.89 and RMSE of 91.48 g/m^2 using canopy height models for grassland AGB. Again, the predicted mean and standard deviation of our predictions consistently fell below the actual field values across most habitat types, indicating that the model also struggled to capture the full range of biomass variability. Additionally, both Lussem et al. (2019) and Zhang et al. (2018) focused exclusively on grasslands, which exhibit lower variability and are less complex to model than, for example, forest understory herbaceous vegetation.

4.3. Spatial patterns and predictions of HAB across habitats

We estimated an average total HAB density of 1.31 ± 0.83 tons/ha, with shrub HAB accounting for the largest share (1.02 ± 0.79 tons/ha), while herbaceous HAB was substantially lower (0.14 ± 0.10 tons/ha). HAB density varied across land cover types, with shrub-dominated areas exhibiting the highest values (1.83 ± 2.42 tons/ha in low shrub habitats), primarily driven by shrub HAB (1.33 ± 1.89 tons/ha). In contrast, agricultural areas had the highest herbaceous HAB density (0.68 ± 6.43 tons/ha) but comparatively lower shrub HAB (1.00 ± 13.19 tons/ha). Forested habitats had the lowest HAB densities with oak forests at 0.85 ± 1.40 tons/ha and pine forests at 0.94 ± 3.86 tons/ha. These results highlight the variability in HAB distribution, with shrubs dominating overall HAB and agricultural areas supporting more herbaceous growth.

Shrub biomass estimates in similar Mediterranean habitats vary widely. Estornell et al. (2012) reported shrub AGB ranging from 0 to over 10 tons/ha in Quercus-dominated forests in Spain, while Casals et al. (2023) documented woody species AGB between 0.2 and 39.3 tons/ha (median = 8.3 tons/ha) in northeastern Spain. Some studies report even higher values: Merino et al. (1990) documented 21.9 tons/ha for heathers in southeastern Andalusia, and Pasalodos-Tato et al. (2015) reported an average of 24.99 tons/ha for heathers, with a regional average of 16.7 tons/ha shrub biomass in Andalusia. Basanta (1982) observed 28.9 tons/ha in mountainous Andalusia. In northern Portugal, Enes et al. (2020) found shrub AGB between 0.12 and 28.88 tons/ha, with biomass increasing post-fire. Their species composition (e.g., *Cistus* spp., *Erica* spp., *Genista* spp., and *Ulex* spp.) closely matches ours, and post-fire plots within our study area ranged from 1 to 5 tons/ha (Enes et al., 2020). Similarly, Aranha et al. (2020) reported post-fire biomass accumulation exceeding 14 tons/ha within 10 years, with an average of 18.3 tons/ha in Northwest Portugal and 7.7 tons/ha in the Northeast. However, all of those studies estimated traditional total biomass, with the aim of assessing for example fire hazard or carbon stocks, while our aim was considerably different to focus on plant biomass accessible as forage to herbivore species, explaining our much lower values.

Nevertheless, both the total and shrub HAB models predicted HAB across the study area with considerably high certainty. The average CV of the total and shrub HAB predictions were 27.08 % and 32.53 %, respectively, indicating lower uncertainty compared to other studies, e.g. ranging from 40 % to 100 % for shrub biomass predictions (Greaves et al., 2016) or from 121 % to 136 % for total biomass and from 148 % to 190 % for shrub biomass (Li et al., 2017). Additionally, it needs to be considered that biomass model fitting errors generally decrease with increasing plot size or spatial resolution, partly due to reduced edge effects but mainly because biomass values become less variable at larger spatial scales (Duncanson et al., 2020). Our fitting error could therefore also be related to the high resolution of our data.

5. Conclusions and pathways for improved biomass monitoring

Our study underscores the value of integrating spectral and structural remote sensing data for estimating herbivore-accessible biomass, confirming findings from previous research (e.g., Bazzo et al., 2023; Estornell et al., 2012; Greaves et al., 2016). Structural metrics generally outperform spectral indices alone and their combination consistently enhances prediction accuracy. Despite challenges such as environmental heterogeneity and the costs of high-resolution UAV data, LiDAR remains a powerful tool for capturing detailed vegetation structure and enhancing AGB estimation (Bazzo et al., 2023; Greaves et al., 2016). Future advancements in remote sensing technologies and data

accessibility will further support vegetation and AGB mapping efforts (Greaves et al., 2016). However, accurately modeling biomass in complex, heterogeneous environments requires frequent sampling, extensive datasets, and multi-temporal observations across growing seasons and land management regimes to build more generalizable models (Morais et al., 2021; Bazzo et al., 2023). Integrating UAV data with advanced satellite technologies (such as Landsat and GEDI) will enhance biomass estimation, making it more reliable and scalable for environmental monitoring and resource management.

Our modeling framework, using Generalized Additive Mixed Models, provides a scalable and robust solution for HAB estimation in complex ecosystems. It captures non-linear effects, accommodates hierarchical data structures, and addresses the unique characteristics of biomass data, including excess zeros and continuous values, thereby overcoming limitations of traditional linear models. While GAMMs can be computationally more demanding than machine-learning approaches such as Random Forests or Boosted Regression Trees, particularly when fitting complex smooth terms or random effects, they remain tractable for datasets of the size used here. For larger-scale applications computation could be accelerated by pre-selecting variables or using coarser predictor layers. Importantly, GAMMs allow direct incorporation of ecological structure and yield interpretable functional relationships, making them especially valuable for ecological inference and management applications. Moreover, this framework is adaptable to other regions and ecosystems, provided that the hierarchical structure of the data and the range of predictor variables are carefully considered. This allows the extension of HAB estimation across different spatial and ecological contexts, providing an important foundation for advancing herbivore ecology research, informing habitat management, and guiding conservation strategies in this ecologically complex landscape.

CRediT authorship contribution statement

Annika M. Zuleger: Writing – original draft, Methodology, Investigation, Formal analysis, Data curation, Conceptualization. **Martina M. Viti:** Writing – review & editing, Methodology, Investigation. **Luise Quoss:** Writing – review & editing, Software, Investigation, Data curation. **Filipe S. Dias:** Writing – review & editing, Formal analysis. **Luís Borda-de-Água:** Writing – review & editing, Formal analysis. **Miguel N. Bugalho:** Writing – review & editing, Supervision, Methodology, Conceptualization. **Henrique M. Pereira:** Writing – review & editing, Supervision, Methodology, Investigation, Funding acquisition, Formal analysis, Data curation, Conceptualization.

Declaration of competing interest

The authors declare that they have no known competing financial interests or personal relationships that could have appeared to influence the work reported in this paper.

Acknowledgements

We would like to thank the Peneda-Gerês National Park, as well as the Institute for Nature Conservation and Forests, Portugal (ICNF) for the support and permission to conduct our monitoring initiative and fieldwork. Further, we thank everyone who helped with the fieldwork and collecting the biomass data, especially Joel Neves, Kim Kaufmann and the MSc students from the Martin-Luther-University. Moreover, we would like to thank CIBIO in Vairão, especially Rita Seabra, for allowing us to use their drying chambers to dry our biomass samples during fieldwork, without which this work would not have been possible, and Theresa Jörger-Hickfang and Maria Mendez for organizing this collaboration last minute.

This work was supported by the German Centre for Integrative Biodiversity Research (iDiv) Halle-Jena-Leipzig, funded by the German Research Foundation (FZT 118).

Appendix A. Supplementary data

Supplementary data to this article can be found online at https://doi.org/10.1016/j.srs.2025.100302.

Data availability

Data (CSV tables required for analysis) and R scripts for the statistical analysis are available on GitHub under https://github.com/AMZuleger/Mapping_herbivore-accessible_biomass_UAV and Zenodo under https://doi.org/10.5281/zenodo.17347321. All remote sensing and GIS data is available on Zendodo under https://doi.org/10.5281/zenodo.17348401.used for this analysis, including the LiDAR point cloud data is available on Zenodo under https://doi.org/10.5281/zenodo.17348401.

References

AgEagle, 2023. eMotion flight control software [Computer software]. https://ageagle.com/drone-software/emotion/.

Anderson, K.E., Glenn, N.F., Spaete, L.P., Shinneman, D.J., Pilliod, D.S., Arkle, R.S., McIlroy, S.K., Derryberry, D.R., 2018. Estimating vegetation biomass and cover across large plots in shrub and grass dominated drylands using terrestrial lidar and machine learning. Ecol. Indic. 84, 793–802. https://doi.org/10.1016/j.ecolind.2017.09.034.

Aranha, J., Enes, T., Calvão, A., Viana, H., 2020. Shrub biomass estimates in former burnt areas using sentinel 2 images processing and classification. Forests 11 (5), 555. https://doi.org/10.3390/f11050555.

ASPRS, 2019. *LAS 1.4 R15 Specification*. American Society for Photogrammetry and Remote Sensing.

Basanta, A., 1982. Vegetación seral en Sierra Morena. Estudio ecológico de las respuestas del matorral a distintas intervenciones en el Coto Nacional «La Pata del Caballo»(Huelva). Universidad de Sevilla [PhD].

Bazzo, C.O.G., Kamali, B., Hütt, C., Bareth, G., Gaiser, T., 2023. A review of estimation methods for aboveground biomass in grasslands using UAV. Remote Sens. 15 (3), 639. https://doi.org/10.3390/rs15030639.

Breheny, P., Burchett, W., 2017. Visualization of regression models using visreg. The R Journal 9 (2), 56. https://doi.org/10.32614/RJ-2017-046.

Burai, P., Deák, B., Valkó, O., Tomor, T., 2015. Classification of herbaceous vegetation using airborne hyperspectral imagery. Remote Sens. 7 (2), 2046–2066. https://doi.org/10.3390/rs70202046.

Campbell, M.J., Dennison, P.E., Kerr, K.L., Brewer, S.C., Anderegg, W.R.L., 2021. Scaled biomass estimation in woodland ecosystems: testing the individual and combined capacities of satellite multispectral and lidar data. Rem. Sens. Environ. 262, 112511. https://doi.org/10.1016/j.rse.2021.112511.

Carvalho-Santos, C., Monteiro, A., Arenas-Castro, S., Greifeneder, F., Marcos, B., Portela, A., Honrado, J., 2018. Ecosystem services in a protected Mountain range of Portugal: satellite-based products for state and trend analysis. Remote Sens. 10 (10), 1573. https://doi.org/10.3390/rs10101573.

Casals, P., Gabriel, E., De Cáceres, M., Ríos, A.I., Castro, X., 2023. Composition and structure of mediterranean shrublands for fuel characterization. Ann. For. Sci. 80 (1), 23. https://doi.org/10.1186/s13595-023-01190-y.

Castro, H., Freitas, H., 2009. Above-ground biomass and productivity in the montado: from herbaceous to shrub dominated communities. J. Arid Environ. 73 (4–5), 506–511. https://doi.org/10.1016/j.jaridenv.2008.12.009.

Ceballos, A., Hernández, J., Corvalán, P., Galleguillos, M., 2015. Comparison of airborne LiDAR and satellite hyperspectral remote sensing to estimate vascular plant richness in deciduous mediterranean forests of central Chile. Remote Sens. 7 (3), 2692–2714. https://doi.org/10.3390/rs70302692.

Chang, J., Shoshany, M., 2016. Mediterranean shrublands biomass estimation using Sentinel-1 and Sentinel-2. 2016 IEEE International Geoscience and Remote Sensing Symposium (IGARSS), pp. 5300–5303. https://doi.org/10.1109/IGARSS.2016.7730380.

DJI, 2019. DJI terra [Computer software]. https://enterprise.dji.com/de/dji-terra.

Duncanson, L., Neuenschwander, A., Hancock, S., Thomas, N., Fatoyinbo, T., Simard, M., Silva, C.A., Armston, J., Luthcke, S.B., Hofton, M., Kellner, J.R., Dubayah, R., 2020. Biomass estimation from simulated GEDI, ICESat-2 and NISAR across environmental gradients in sonoma county, California. Rem. Sens. Environ. 242, 111779. https://doi.org/10.1016/j.rse.2020.111779.

Estornell, J., Ruiz, L.A., Velázquez-Martí, B., Hermosilla, T., 2012. Estimation of biomass and volume of shrub vegetation using LiDAR and spectral data in a Mediterranean environment. Biomass Bioenergy 46, 710–721. https://doi.org/10.1016/j.biombioe.2012.06.023.

Fassnacht, F.E., Hartig, F., Latifi, H., Berger, C., Hernández, J., Corvalán, P., Koch, B., 2014. Importance of sample size, data type and prediction method for remote sensing-based estimations of aboveground forest biomass. Rem. Sens. Environ. 154, 102–114. https://doi.org/10.1016/j.rse.2014.07.028.

Fernández-Alonso, J.M., Llorens, R., Sobrino, J.A., Ruiz-González, A.D., Alvarez-González, J.G., Vega, J.A., Fernández, C., 2022. Exploring the potential of lidar and Sentinel-2 data to model the post-fire structural characteristics of Gorse shrublands in NW Spain. Remote Sens. 14 (23), 6063. https://doi.org/10.3390/rs14236063.

Gorissen, A., Tietema, A., Joosten, N.N., Estiarte, M., Peuelas, J., Sowerby, A., Emmett, B. A., Beier, C., 2004. Climate change affects carbon allocation to the soil in shrublands. Ecosystems 7 (6). https://doi.org/10.1007/s10021-004-0218-4.

Greaves, H.E., Vierling, L.A., Eitel, J.U.H., Boelman, N.T., Magney, T.S., Prager, C.M., Griffin, K.L., 2016. High-resolution mapping of aboveground shrub biomass in Arctic tundra using airborne lidar and imagery. Rem. Sens. Environ. 184, 361–373. https://doi.org/10.1016/j.rse.2016.07.026.

Jakimow, B., Janz, A., Thiel, F., Okujeni, A., Hostert, P., Van Der Linden, S., 2023. EnMAP-Box: imaging spectroscopy in QGIS. SoftwareX 23, 101507. https://doi.org/10.1016/j.softx.2023.101507.

Lefsky, M.A., Cohen, W.B., Parker, G.G., Harding, D.J., 2002. Lidar remote sensing for ecosystem studies. Bioscience 52 (1), 19. https://doi.org/10.1641/0006-3568(2002)052%255B0019:LRSFES%255D2.0.CO, 2.

Lei, T., Pang, Z., Wang, X., Li, L., Fu, J., Kan, G., Zhang, X., Ding, L., Li, J., Huang, S., Shao, C., 2016. Drought and carbon cycling of grassland ecosystems under global change: a review. Water 8 (10), 460. https://doi.org/10.3390/w8100460.

Li, A., Dhakal, S., Glenn, N., Spaete, L., Shinneman, D., Pilliod, D., Arkle, R., McIlroy, S., 2017. Lidar aboveground vegetation biomass estimates in shrublands: prediction, uncertainties and application to coarser scales. Remote Sens. 9 (9), 903. https://doi.org/10.3390/rs9090903.

Lindsay, J.B., 2016. Whitebox GAT: a case study in geomorphometric analysis. Comput. Geosci. 95, 75–84. https://doi.org/10.1016/j.cageo.2016.07.003.

Lourenço, J., Quental, N., 2007. Naturbanization and sustainability in the National Park of Peneda-gerês. Proceedings of the International Workshop on Naturbanization in National Parks at Sierra Nevada National Park. https://hdl.handle.net/1822/8778.

Lowe, D.G., 1999. Object recognition from local scale-invariant features. Proceed. Seventh IEEE Int. Conf. Computt. Vision 2, 1150–1157. https://doi.org/10.1109/ICCV.1999.790410.

Lussem, U., Bolten, A., Menne, J., Gnyp, M.L., Schellberg, J., Bareth, G., 2019. Estimating biomass in temperate grassland with high resolution canopy surface models from UAV-Based RGB images and vegetation indices. J. Appl. Remote Sens. 13 (3), 1. https://doi.org/10.1117/1.JRS.13.034525.

Manfreda, S., McCabe, M.F., Miller, P.E., Lucas, R., Pajuelo Madrigal, V., Mallinis, G., Ben Dor, E., Helman, D., Estes, L., Ciraolo, G., Müllerová, J., Tauro, F., De Lima, M.I., De Lima, J.L.M.P., Maltese, A., Frances, F., Caylor, K., Kohv, M., Perks, M., et al., 2018. On the use of unmanned aerial systems for environmental monitoring. Remote Sens. 10 (4), 641. https://doi.org/10.3390/rs10040641.

Marra, G., Wood, S.N., 2011. Practical variable selection for generalized additive models. Comput. Stat. Data Anal. 55 (7), 2372–2387. https://doi.org/10.1016/j.csda.2011.02.004.

Merino, O., Martin, M.P., Martin, A., Merino, J., 1990. Successional and temporal changes in primary productivity in two mediterranean scrub ecosystems. Acta Oecol. 11 (1), 103–112.

Morais, T.G., Teixeira, R.F.M., Figueiredo, M., Domingos, T., 2021. The use of machine learning methods to estimate aboveground biomass of grasslands: a review. Ecol. Indic. 130, 108081. https://doi.org/10.1016/j.ecolind.2021.108081.

Narine, L.L., Popescu, S.C., Malambo, L., 2019. Synergy of ICESat-2 and landsat for mapping forest aboveground biomass with deep learning. Remote Sens. 11 (12), 1503. https://doi.org/10.3390/rs11121503.

NASA/METI/AIST/Japan Spacesystems And U.S./Japan ASTER Science Team, 2019. ASTER global digital elevation model V003. NASA EOSDIS Land Processes Distributed Active Archive Center. https://doi.org/10.5067/ASTER/ASTGTM.003.

Pasalodos-Tato, M., Ruiz-Peinado, R., Del Río, M., Montero, G., 2015. Shrub biomass accumulation and growth rate models to quantify carbon stocks and fluxes for the mediterranean region. Eur. J. For. Res. 134 (3), 537–553. https://doi.org/10.1007/s10342-015-0870-6.

Pervin, R., Robeson, S.M., MacBean, N., 2022. Fusion of airborne hyperspectral and LiDAR canopy-height data for estimating fractional cover of tall woody plants, herbaceous vegetation, and other soil cover types in a semi-arid savanna ecosystem. Int. J. Rem. Sens. 43 (10), 3890–3926. https://doi.org/10.1080/01431161.2022.2105176.

Pix4D, 2011. Postflight terra 3D [Computer software]. https://d3pcsg2wjq9izr.cloudfront.net/files/65969/download/483237/14-sensefly-postflight.pdf.

Pix4D, 2023. Pix4Dmapper [Computer software]. https://www.pix4d.com/product/pix4dmapper-photogrammetry-software/.

Riquelme, L., Duncan, D.H., Rumpff, L., Vesk, P.A., 2022. Using remote sensing to estimate understorey biomass in semi-arid woodlands of south-eastern Australia. Remote Sens. 14 (10), 2358. https://doi.org/10.3390/rs14102358.

Rodrigues, P., 2010. Landscape changes in castro laboreiro: from farmland abandonment to forest regeneration (Issue. https://repositorio.ul.pt/bitstream/10451/2302/1/ulfc08095_tm_Patricia_Rodrigues.pdf.

Roussel, J.-R., Auty, D., 2016. lidR: airborne LiDAR data manipulation and visualization for forestry applications (p. 4.1.2). https://doi.org/10.32614/CRAN.package.lidR.

van der Zanden, E.H., Carvalho-Ribeiro, S.M., Verburg, P.H., 2018. Abandonment landscapes: user attitudes, alternative futures and land management in Castro Laboreiro, Portugal. Reg. Environ. Change 18 (5), 1509–1520. https://doi.org/10.1007/s10113-018-1294-x.

Vega, J.A., Arellano-Pérez, S., Álvarez-González, J.G., Fernández, C., Jiménez, E., Fernández-Alonso, J.M., Vega-Nieva, D.J., Briones-Herrera, C., Alonso-Rego, C., Fontúrbel, T., Ruiz-González, A.D., 2022. Modelling aboveground biomass and fuel load components at stand level in shrub communities in NW Spain. For. Ecol. Manag. 505, 119926. https://doi.org/10.1016/j.foreco.2021.119926.

Wang, C.T., Long, R.J., Wang, Q.J., Ding, L.M., Wang, M.P., 2007. Effects of altitude on plant-species diversity and productivity in an alpine meadow, Qinghai—Tibetan plateau. Aust. J. Bot. 55 (2), 110. https://doi.org/10.1071/BT04070.

Wood, S.N., 2011. Fast stable restricted maximum likelihood and marginal likelihood estimation of semiparametric generalized Linear models. J. Roy. Stat. Soc. B Stat. Methodol. 73 (1), 3–36. https://doi.org/10.1111/j.1467-9868.2010.00749.x.

Zhang, H., Sun, Y., Chang, L., Qin, Y., Chen, J., Qin, Y., Du, J., Yi, S., Wang, Y., 2018. Estimation of Grassland canopy height and aboveground biomass at the quadrat Scale using unmanned aerial vehicle. Remote Sens. 10 (6), 851. https://doi.org/10.3390/rs10060851.

Zhao, Y., Liu, X., Wang, Y., Zheng, Z., Zheng, S., Zhao, D., Bai, Y., 2021. UAV-based individual shrub aboveground biomass estimation calibrated against terrestrial LiDAR in a shrub-encroached grassland. Int. J. Appl. Earth Obs. Geoinf. 101, 102358. https://doi.org/10.1016/j.jag.2021.102358.

Pereira, H. M., & Navarro, L. M. (Hrsg.). (2015). *Rewilding European Landscapes*. Springer International Publishing.